Thermally Crosslinkable Hole-Transporting Poly(fluorene-*co*-triphenylamine) for Multilayer Polymer Light-Emitting Diodes

WEN-FEN SU,[1] RUEI-TANG CHEN,[2] YUN CHEN[1]

[1]Department of Chemical Engineering, National Cheng Kung University, Tainan, Taiwan

[2]Nanopower and Thin Film Technology Center, ITRI South, Industrial Technology Research Institute, Tainan, Taiwan

Received 18 August 2010; accepted 27 September 2010
DOI: 10.1002/pola.24432
Published online 18 November 2010 in Wiley Online Library (wileyonlinelibrary.com).

ABSTRACT: This article reports the synthesis and characterization of a novel thermally crosslinkable hole-transporting poly (fluorene-*co*-triphenylamine) (PFO-TPA) by Suzuki coupling reaction, followed with its application in the fabrication of multilayer light-emitting diodes by wet processes. The thermal, photophysical, and electrochemical properties of PFO-TPA were investigated by differential scanning calorimeter, thermogravimetric analysis, optical spectroscopy, and cyclic voltammetry, respectively. Thermally crosslinked PFO-TPA, through pendant styryl groups, demonstrates excellent thermal stability ($T_d > 400$ °C, $T_g = 152$ °C), solvent resistance, and film homogeneity. Its highest occupied molecular orbital level (−5.30 eV) lies between those of PEDOT:PSS (−5.0 ∼ −5.2 eV) and poly(9,9-dioctylfluorene) (PFO: −5.70 eV), forming a stepwise energy ladder to facilitate hole injection. Multilayer device with crosslinked PFO-TPA as hole-injection layer (HIL) (ITO/PEDOT:PSS/HIL/PFO/LiF/Ca/Al) was readily fabricated by successive spin-coating processes, its maximum luminance efficiency (3.16 cd/A) were about six times higher than those without PFO-TPA layer (0.50 cd/A). The result of hole-only device also confirmed hole-injection and hole-transport abilities of crosslinked PFO-TPA layer. Consequently, the device performance enhancement is attributed to more balanced charges injection in the presence of crosslinked PFO-TPA layer. The thermally crosslinkable PFO-TPA is a promising material for the fabrication of efficient multilayer polymer light-emitting diodes because it is not only a hole-transporting polymer but also thermally crosslinkable. © 2010 Wiley Periodicals, Inc. J Polym Sci Part A: Polym Chem 49: 352–360, 2011

KEYWORDS: crosslinking; hole injection; hole-transporting polymer; morphology; multilayer light-emitting diodes; synthesis; thermally crosslinkable polymer

INTRODUCTION Polymer light-emitting diodes (PLEDs) have attracted much attention in the last two decades because of their potential applications in large-area flat panel displays and solid-state lighting.[1–5] Organic materials in PLEDs have some advantages such as potentially low cost, facile processing by spin-coating and ink-jet printing methods. However, single-layer PLEDs usually exhibit limited device performance. The major drawback of single layer PLEDs is unbalanced transport and injection of charge carriers. To solve this problem, fabricating multilayer device is usually necessary by inserting hole-transporting (or injecting) layer (HTL) or electron-transporting (or injecting) layer,[6–11] or the hole-transporting moieties such as triphenylamine or carbazole introduce on the polymer chain.[12,13] Several multilayer devices were fabricated by the solution processing method,[7,14–16] strict selection of solvents and processing conditions were crucial to prevent redissolution of previous layers.

One way to increase solvent resistance of a polymer is to increase its crosslinking density, which can be attained by thermal[17–26] or photo-excited[27–32] reactions. For example, Kim and coworkers[26] synthesized a new thermally curable triarylamine containing terminal trifluorovinyl ether groups, which was thermally cured to demonstrate excellent solvent resistance, high thermal stability, high transparency, and good surface smoothness. Jen and coworkers[23] reported thermally crosslinkable HTLs derived from *N*,*N*′-bis(tolyl)-*N*,*N*′-diphenyl-1,1′-biphenyl-4,4′-diamine and *N*,*N*′-bis(1-napthyl)-*N*,*N*′-diphenyl-1,1′-biphenyl-4,4′-diamine by incorporating styryl groups. Reynolds and coworkers[21] prepared a hyperbranched polymer with subsequently polymerizable vinyl groups at the periphery; its thermal polymerization afforded insoluble films, on which a light-emitting polymer could be spun cast. An optimal HTM should possess high solvent resistance to enable successive spin coating and proper highest occupied molecular orbital (HOMO) energy level [lying between ITO and emitting layer (EML)] to facilitate hole injection. Tamoto and coworkers[33] indicated that the HOMO level of HTM was the dominant factor to obtain high performance and durability in organic PLEDs. For instance, owing to its appropriate HOMO level (−5.3 eV), poly[(9,9-dioctylfluorenyl-2,7-diyl)-co-(4,4′-(*N*-(4-*sec*-butylphenyl))diphenylamine)] (TFB) was successfully used as HIL and HTL between a poly(styrenesulphonate)-doped poly(3,4-ethylenedioxythiophene) (PEDOT:PSS) and an EML to

Correspondence to: R.-T. Chen (E-mail: raychen@itri.org.tw) or Y. Chen (E-mail: yunchen@mail.ncku.edu.tw)
Journal of Polymer Science: Part A: Polymer Chemistry, Vol. 49, 352–360 (2011) © 2010 Wiley Periodicals, Inc.

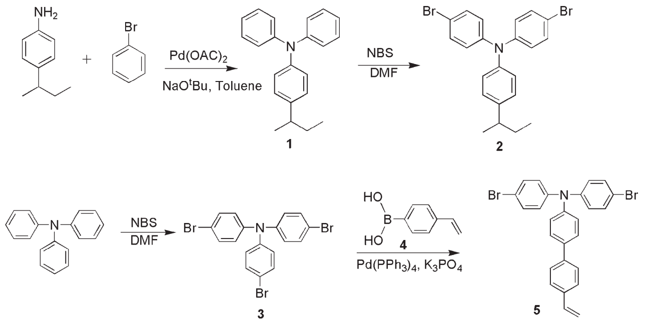

SCHEME 1 Synthesis of Monomers **2** and **5**.

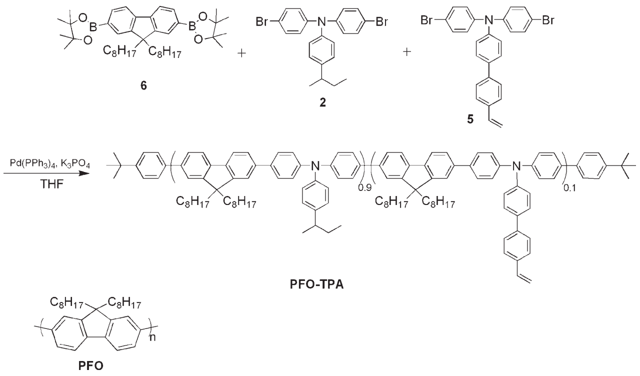

SCHEME 2 Synthesis of random copolymer PFO-TPA and structure of PFO.

substantially improve the device efficiency of multilayer PLEDs.[7,14] However, although the enhancing effect of the TFB on multilayer PLEDs was demonstrated, the TFB layer may be redissolved during subsequent spin coating because of its poor solvent resistance. Therefore, the actual TFB thickness in the device cannot be controlled at will. This may lead to poor reproducibility in the fabrication of multilayer devices by solution processes.

This article presents a method to solve this problem, that is, synthesizing a new thermally crosslinkable hole-transporting copolymer [poly(fluorene-*co*-triphenylamine) (PFO-TPA)] by incorporating thermally reactive styryl groups. The PFO-TPA is expected to enhance device efficiency because of its structural similarity to the TFB. Moreover, its thermal crosslinking will improve thermal and chemical stabilities and film-forming property. In addition, fabrication of multilayer PLEDs with PFO-TPA as hole-injection layer (HIL) is readily obtainable by successive spin-coating processes and will be highly reproducible because of its thermal crosslinking ability. Current results reveal that crosslinked PFO-TPA layer effectively enhances emission efficiency of multilayer PLED devices. In addition, introducing thermally crosslinkable groups to emitting copolyfluorenes is an effective way to improve their processability, thermal stability, and film morphology.

RESULT AND DISCUSSION

Synthesis and Characterization of Monomers and Polymer

Scheme 1 illustrates the synthetic routes of the monomers (**2**, **5**). 9,9-Dioctylfluorene-2,7-diboronic acid bispinacol ester,[34–36] 4-(3-methylpropyl)-*N*,*N*-bis(4-bromophenyl)aniline (**2**),[37,38] and tri(4-bromophenyl)amine (**3**)[39] were prepared according to the procedures reported previously. The monomer *N*,*N*-bis(4-bromophenyl)-*p*-(4-vinylphenyl)aniline (**5**) with styryl moiety was successfully synthesized from triphenylamine in two steps. Bromination of triphenylamine with *N*-bromosuccinimide led to tri(4-bromophenyl)amine (**3**), which further coupled with *p*-vinylphenylboronic acid (**4**) to obtain monomer **5**. Monomers **2** and **5** were purified by repeat recrystallization before polymerization. Chemical structure of **5** was satisfactorily confirmed by ^{1}H NMR, ^{13}C NMR spectra, elemental analysis (EA), and mass spectrometry. Poly(9,9-dioctylfluorene) (PFO) and PFO-TPA with reactive styryl groups were successfully synthesized by the Suzuki coupling reaction using $Pd(PPh_3)_4$ as the catalyst (Scheme 2), the monomer molar ratio for PFO-TPA was **6**:**2**:**5** = 1:0.9:0.1 (5 mol % of **5**). The PFO-TPA and PFO are soluble in common organic solvents such as toluene, THF, and chloroform. Figure 1 shows the ^{1}H NMR spectrum of PFO-TPA in which the chemical shifts at 5.26–5.80 ppm (a) and 6.72–6.80 ppm (b) have been assigned to protons of vinyl substituents ($CH_2{=}CH{-}$). The ratio of peak area of $={CH_2}$ (a) over that of $={CH}{-}$ (b) is roughly 2/1, consistent with the structure of PFO-TPA. The characteristic chemical shifts at 5.26–5.80 ppm indicate the existence of styryl groups, from which thermally crosslinkable character can be expected. The actual composition of pendant vinyl groups is 3.5 mol %, calculated from the area ratio of the peaks at 5.26–5.80 ppm ($={CH_2}$ from monomer **5**) and 2.04 ppm ($-CH_2$ from monomer **6**). The structure of PFO-TPA was satisfactorily characterized by its ^{1}H NMR, ^{13}C NMR spectra, and EA. As shown in Table 1, the weight-average molecular weight (M_w) of PFO-TPA and PFO, determined by gel permeation chromatography (GPC) using polystyrene as standard, were 7.1×10^4 and 14.4×10^4 g/mol, with the polydispersity indexes being 2.0 and 1.8, respectively.

Thermal Crosslinking and Thermal Properties of PFO-TPA

Crosslinked polymers generally reveal enhanced thermal stability which is essential to extend the life time of optoelectronic devices. Low thermal stability in active polymer

TABLE 1 Polymerization Results and Thermal Properties of PFO and PFO-TPA

Polymer	M_n (10^4) (g/mol)[a]	M_w (10^4) (g/mol)[a]	PDI[a]	ΔH (J/g)[b]	T_g (°C)[b]	T_d (°C)[c]
PFO	7.2	14.4	2.0	–	68	432
PFO-TPA	3.9	7.1	1.8	32.8	153	416

[a] Determined by gel permeation chromatography using polystyrene as calibration standard.

[b] Determined by differential scanning calorimetry (DSC) at a heating rate of 10 °C/min.

[c] The temperature at 5 wt % loss in nitrogen atmosphere, measured by TGA.

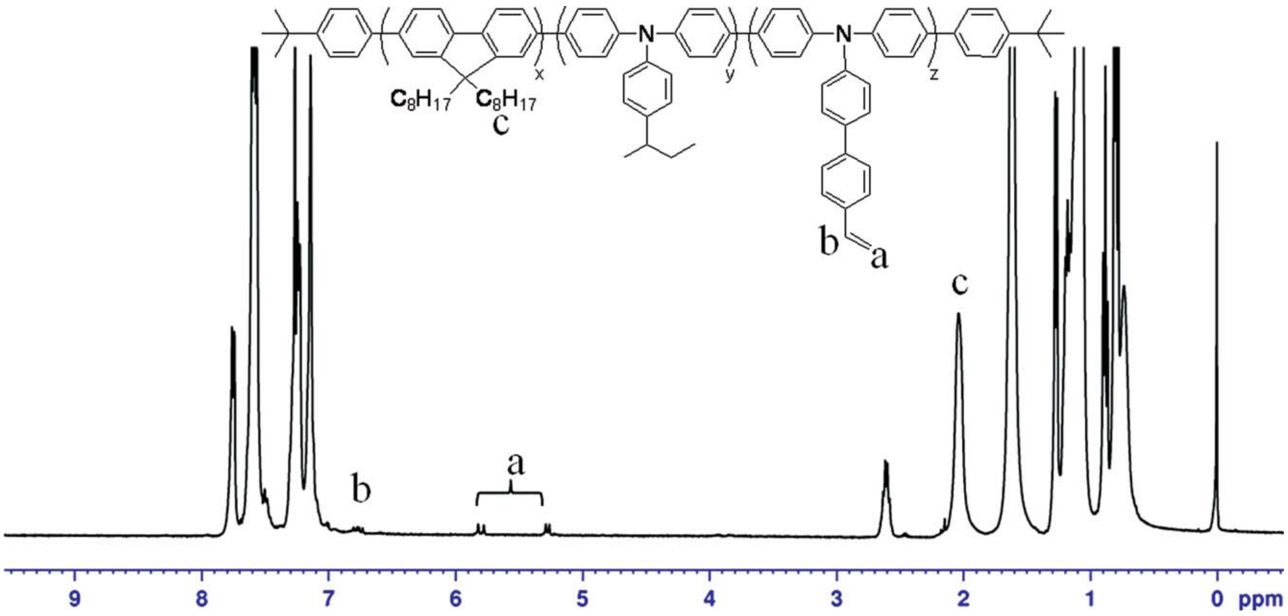

FIGURE 1 The ^{1}H NMR spectrum of PFO-TPA dissolved in $CDCl_3$. The chemical shifts are reported in ppm using tetramethylsilane (TMS) as an internal standard. [Color figure can be viewed in the online issue, which is available at wileyonlinelibrary.com.]

layer leads to severe morphology changes under device operation, which is one of the main causes of device degradation.[40] Thermal resistant and thermal crosslinking characteristics of PFO-TPA were studied by thermogravimetric analysis (TGA) and differential scanning calorimeter (DSC), respectively. The thermal decomposition temperatures (T_d) of PFO and PFO-TPA are above 400 °C (Table 1), indicating they are thermally stable. Thermal crosslinking conditions of PFO-TPA were determined by a similar DSC heating scan to 250 °C. As shown in Figure 2, in the first heating scan, the DSC trace shows a glass transition temperature (T_g) at 152 °C and an exothermic peak at 215 °C, in which the exotherm starts at about 180 °C. The heat released (32.8 J/g) is attributable to crosslinking reaction of the pendant styryl groups. However, on the second heating, no detectable exothermic peak is observed, indicating that most of the styryl groups have been reacted during the first heating scan. Furthermore, the cured PFO-TPA exhibits a slightly raised T_g of 153 °C and no detectable crystallization and melting transitions, suggesting that it is basically an amorphous material. The high T_g is highly desirable to prevent the crystallization process during device operation or thermal annealing, which deteriorates long-term morphological stability. As shown in the inset of Figure 2, the exothermic thermal crosslinking of PFO-TPA under 200 °C is completed within 10 min. This can be confirmed by the absence of exothermic peak in the DSC trace of the crosslinked sample. To ensure complete crosslinking in the following study, the crosslinking of all PFO-TPA films was conducted at 200 °C for 10 min under nitrogen atmosphere.

Optical and Electrochemical Properties

A major challenge needs to be solved for the fabrication of multilayer PLEDs by solution processes, that is, previously deposited layer should be resistant to the following coating solutions. Solvent resistance of the thermally crosslinked PFO-TPA film (200 °C, 10 min) was evaluated by the absorption spectral change before and after rinsing with toluene, which is a good solvent for the film. The absorption maximum and photoluminescence (PL) maximum of pristine PFO-TPA film was located at 386 nm and 438 nm (Table 2), respectively. The absorption spectral variation of the crosslinked PFO-TPA film is negligible after rinsing with toluene (Fig. 3), indicating that the crosslinked PFO-TPA is highly solvent resistant after thermal crosslinking. This characteristic makes it suitable for the fabrication of multilayer PLEDs

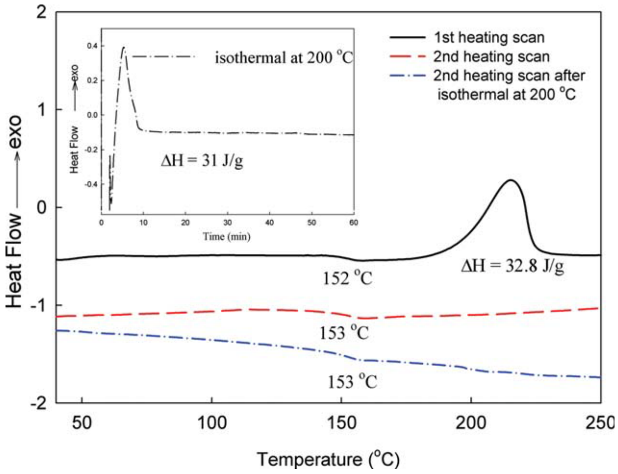

FIGURE 2 DSC traces of PFO-TPA at a heating rate of 10 °C/min. The first scan was used to observe the reaction heat of styryl groups. Inset figure shows isothermal DSC trace at 200 °C. [Color figure can be viewed in the online issue, which is available at wileyonlinelibrary.com.]

TABLE 2 Photophysical Properties of PFO-TPA Film

PFO-TPA	UV–vis λ_{max} (nm)	PL λ_{max} (nm)[a]
Pristine	386	438 (460)[b]
Crosslinked[c]	386	461 (438)
Crosslinked[c] (after toluene rinse)	385	461 (438)

[a] The excitation wavelength was 385 nm.

[b] The values in the parentheses are the PL λ_{max} of the shoulder.

[c] Thermally crosslinked at 200 °C for 10 min under nitrogen atmosphere.

by solution processes. However, the PL intensity of the shoulder at 461 nm is enhanced obviously to become as major peak after the crosslinking, with the original peak at 438 nm remaining almost unchanged (Fig. 3, Table 2). This result suggests that aggregate is formed during the thermal treatment at 200 °C (about 50 °C above the glass transition). This also reflects on the slight broadening of the emission band after the thermal treatment.

Cyclic voltammetry (CV) has been applied and considered as an effective tool to investigate electrochemical properties of conjugated polymers.[41,42] The HOMO that corresponds to ionization potential can be estimated from the onset oxidation potential (E_{ox}) revealed in CV, by the equation $E_{HOMO} = -(E_{ox} + 4.8)$ eV. An ITO glass coated with PFO-TPA thin film was used as the working electrode, supporting in 0.10 M tetra-*n*-butylammonium perchlorate $(n\text{-Bu})_4NClO_4$ in anhydrous acetonitrile. Figure 4(a) shows the cyclic voltammograms of the crosslinked PFO-TPA film. The onset oxidation potential is observed at 0.97 V, which is similar to the 0.95 V of pristine film. Clearly, pendant styryl groups exert only slight affect on the electrochemical property of PFO-TPA film. The HOMO level is estimated to be −5.30 eV. The lowest unoccupied molecular orbital level is estimated to be −2.40 eV, using the HOMO level and the optical band gap (E_g) calculated from onset absorption (Table 3). As shown in Figure 4(b), the HOMO level of crosslinked PFO-TPA (−5.30 eV) lies between those of PEDOT:PSS (−5.0 ~ −5.2 eV)[43] and PFO (−5.70 eV),[44] forming a cascade of HOMO levels. The cascade HOMO levels are highly desirable to promote hole injection in PLED devices. As the PFO-TPA is readily crosslinked by thermal treatment to obtain solvent resistant film, the subsequent spin coating of EML is possible. Therefore, multilayer PLEDs possessing a HOMO cascade can be readily fabricated to enhance device performance. To conclude, the thermally crosslinkable PFO-TPA is a promising hole-injection material applicable in the fabrication of multilayer PLEDs by solution processes.

Surface Morphology of PFO-TPA Film

To achieve efficient emission in PLEDs, it is imperative to obtain highly homogeneous film for each layer. The surface roughness of PFO-TPA spin coated onto ITO was investigated using an atomic force microscope (AFM) and the thickness was 55 nm. As shown in Figure 5, the thermally crosslinked PFO-TPA (200 °C, 10 min) demonstrates a uniform surface morphology with no observable pinhole or aggregate. The root-mean-square (RMS) roughness of the surface is 0.7 nm, which is lower than that of pristine film (RMS = 1.0 nm). This surface smoothing is attributable to the thermal treatment during crosslinking at 200 °C (about 50 °C above the glass transition temperature). This characteristic provides an useful method to smooth the rough surface of previous layers, including ITO glass substrate whose RMS roughness is usually ~3 nm.[23] To conclude, the PFO-TPA exhibits excellent surface morphology after thermal crosslinking, which is a crucial factor in obtaining high-performance PLED devices.

Optoelectronic Properties of LED Devices Using PFO-TPA As Hole-Injection Layer

Multilayer PLEDs [ITO/PEDOT:PSS (30 nm)/PFO-TPA (55 nm)/PFO (92 nm)/Ca (50 nm)/Al (100 nm)] were fabricated by successive spin coating to investigate their emission performance. When the PFO-TPA layer was not thermally crosslinked, the reproducibility of device performance was very poor (Table 4), because of partial re-dissolution of PFO-TPA film during spin coating of the emitting PFO layer. Therefore, thermally crosslinked PFO-TPA and poly(9,9-dioctylfluorene) (PFO) were used as HIL and EML, respectively. The maximum brightness and maximum current efficiency of the device (5820 cd/m^2, 0.57 cd/A) are superior to those without the HIL layer (2160 cd/m^2, 0.18 cd/A). Inserting the crosslinked PFO-TPA as HIL significantly enhances the current efficiency (0.18 cd/A → 0.57 cd/A). This is attributed to improve hole injection because of the hole-transporting triphenylamine groups in crosslinked PFO-TPA, whose HOMO level forms a stepwise energy ladder with those of PEDOT and PFO. To improve the EL performance, a device with extra lithium fluoride (LiF) layer was also fabricated to balance electron injection; the device configuration is ITO/PEDOT:PSS (30 nm)/HIL (55 nm)/PFO (92 nm)/LiF (1 nm)/Ca (50 nm)/Al (100 nm). Figure 6 shows its current density versus bias and brightness versus bias curves (*J*–*B*–*V*), with the characteristic data summarized in Table 4. The turn-on voltage (at 10 cd/m^2), maximum brightness, and maximum

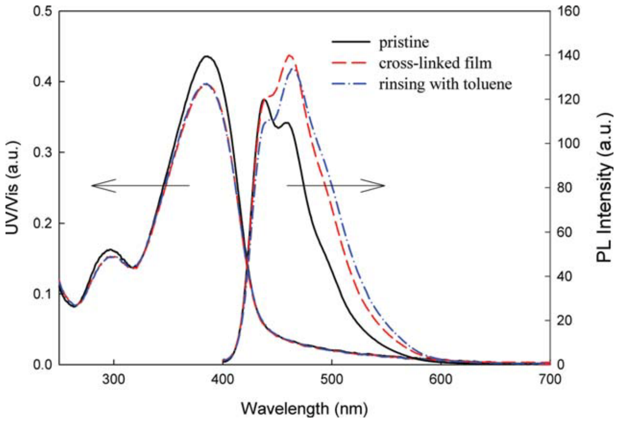

FIGURE 3 Absorption and photoluminescence (PL) spectra (λ_{ex}: 385 nm) of PFO-TPA films: (—) pristine film; (– – –) thermally crosslinked film; (–·–) crosslinked film after toluene rinse.

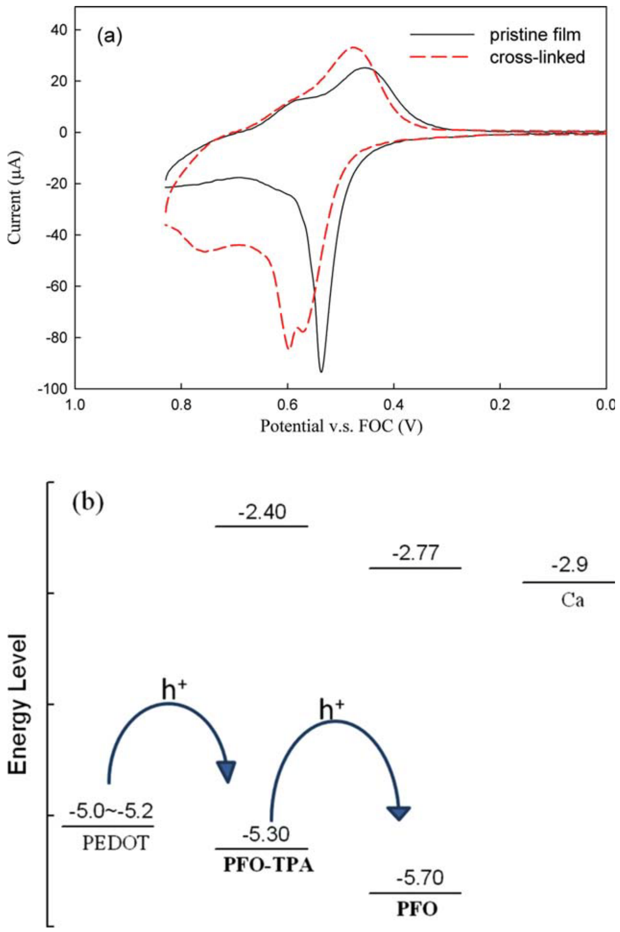

FIGURE 4 (a) Cyclic voltammograms of thermally crosslinked PFO-TPA at a scan rate of 100 mV/s; (b) Energy level diagrams of PEDOT, PFO-TPA, and PFO. [Color figure can be viewed in the online issue, which is available at wileyonlinelibrary.com.]

TABLE 3 Electrochemical Properties of PFO-TPA and PFO

	E_{ox} vs. Ag/Ag$^+$ (V)[a]	E_{ox} vs. FOC (V)[b]	E_{HOMO} (eV)[c]	E_{LUMO} (eV)[d]	E_g^{opt} (eV)[e]
PFO	1.37	0.90	−5.70	−2.77	2.93
PFO-TPA	0.97	0.50	−5.30	−2.40	2.90

[a] Onset oxidation potential obtained from cyclic voltammograms.

[b] $E_{FOC} = 0.47$ V vs. Ag/AgCl.

[c] $E_{HOMO} = -(E_{ox,FOC} + 4.8\ \text{V})$ eV.

[d] $E_{LUMO} = E_g + E_{HOMO}$.

[e] Band gaps obtained from onset absorption (λ_{onset}): $E_g = 1240/\lambda_{onset}$.

current efficiency are 4.6 V, 6140 cd/m^2, and 3.16 cd/A, respectively. However, the turn-on voltage of the device without the HIL layer is 5.1 V, with maximum brightness and maximum current efficiency being only 2410 cd/m^2 and 0.50 cd/A. Moreover, the performance of the crosslinked PFO-TPA-based device surpasses that based on non-crosslinked PFO-TPA as HIL layer (Table 4). Clearly, inserting a thermally crosslinked PFO-TPA as HIL and LiF as electron-injection layer significantly enhances the current efficiency from 0.50 cd/A to 3.16 cd/A. The enhancement is mainly attributed to increased hole- and electron-injection abilities that facilitate more balanced charges injection. The current efficiency (3.16 cd/A) is even higher than 1.96 cd/A of the device fabricated by using highly purified PFO as EML.[45] The multilayer device reveals EL emission peaked at 437 nm corresponding to $S_{10} \rightarrow S_{00}$ vibronic transition of fluorene segments and minor emissions at 461 nm and 492 nm corresponding to $S_{10} \rightarrow S_{01}$ and $S_{10} \rightarrow S_{02}$ vibronic transitions (Fig. 7). Its EL spectrum is analogous to that of PFO-based device (ITO/PEDOT:PSS/PFO/Ca/Al), suggesting that the emission is originated from emitting PFO layer. To verify the EL emission is mainly contributed from emitting PFO layer, a device using the crosslinked PFO-TPA itself as EML

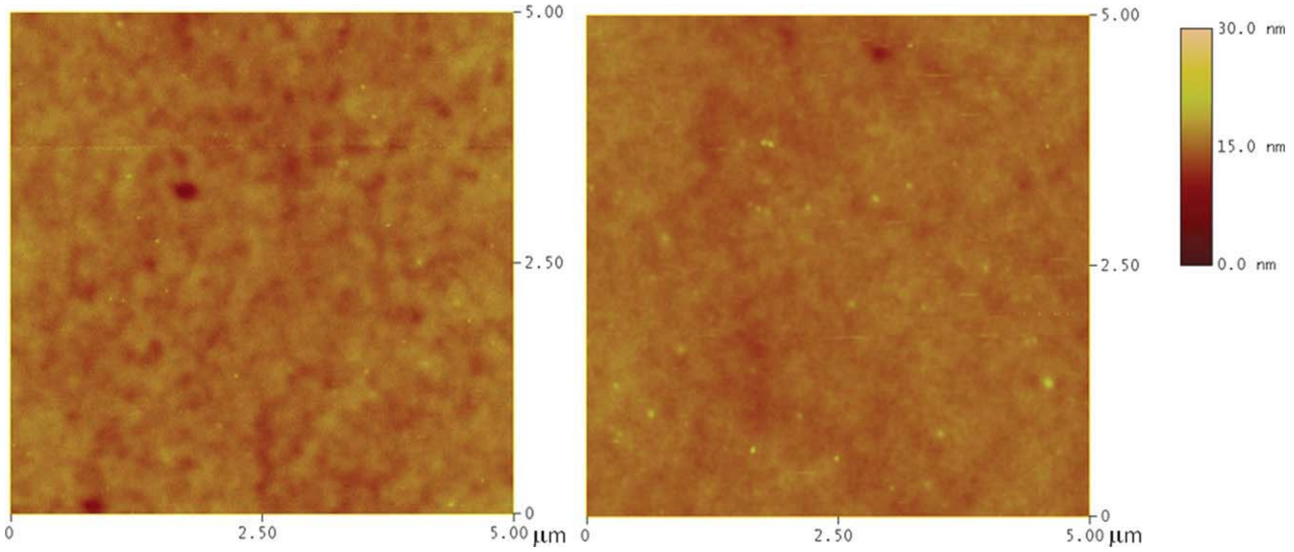

FIGURE 5 AFM images of PFO-TPA films coated on ITO glass: (a) pristine film, RMS roughness = 1.0 nm; (b) after thermally crosslinked at 200 °C for 10 min, RMS roughness = 0.7 nm. [Color figure can be viewed in the online issue, which is available at wileyonlinelibrary.com.]

TABLE 4 Optoelectronic Properties of the PFO-Based PLEDs[a]

HIL	V_{on}[b] (V)	L_{max}[c] (cd/m^2)	LE_{max} (cd/A)[d]	CIE 1931 (x, y)[e]
PFO-TPA noncrosslinked	4.6–4.7[f]	5190–5710[f]	0.72–1.03 (at 4.7–4.9 V)[f]	(0.15, 0.08)–(0.16, 0.08)[f]
PFO-TPA crosslinked	4.6	6140 (at 10.2 V)	3.16 (at 4.9 V)	(0.16, 0.08)
No HIL	5.1	2410 (at 8.0 V)	0.50 (at 5.1 V)	(0,16, 0.08)

[a] Device configuration: ITO/PEDOT:PSS/HIL/PFO/LiF/Ca/Al.

[b] Turn-on voltage: at a luminance of 10 cd/m^2.

[c] Maximum luminance.

[d] Maximum luminance efficiency.

[e] The 1931 CIE coordinates at about 1000 cd/m^2.

[f] The value ranges are those obtained from several experiments due to low reproducibility.

[ITO/PEDOT:PSS (30 nm)/PFO-TPA (55 nm)/Ca/Al] was fabricated to measure its EL emission. The EL spectrum demonstrates main peak at 452 nm and shoulders at 437 and 472 nm, which is very different from that of the multilayer devices (Fig. 7). This result indicates that the electrons and holes mainly recombine in the emitting PFO layer.

To confirm the hole-injection property of crosslinked PFO-TPA, hole-only devices [ITO/PEDOT:PSS/with or without PFO-TPA (55 nm)/PFO (92 nm)/Au (50 nm)/Al (100 nm)] were fabricated to compare their current density characteristics. Figure 8 shows the relationships between current density and electrical field for the hole-only devices. Inserting a crosslinked PFO-TPA layer greatly shifts the curve horizontally to the left, indicating that the crosslinked PFO-TPA HIL effectively increases the device's current density under the same external field. For example, at a field of 8 × 10^5 (V/cm), the current density (ca. 256 mA/cm^2) is about 100 times larger than that without HIL layer (ca. 2.53 mA/cm^2). As a result, it significantly reduces the turn-on electric field (at 10 mA/cm^2) from 11 × 10^5 V/cm to 6 × 10^5 V/cm, which is consistent with the device results obtained above. The results confirm that the thermally crosslinked PFO-TPA layer effectively improves hole-injection ability of the devices.

The mobility of charge carrier is also an important factor in determining the performance of a LED device. To evaluate hole mobility of the thermally crosslinked PFO-TPA, a hole-only device [ITO/PEDOT:PSS (30 nm)/PFO-TPA (55 nm)/Au (50 nm)/Al (100 nm)] was fabricated and its current–voltage curves fitted to the space charge limited current model.[46–48] The estimated hole mobility (μ) of the thermally crosslinked PFO-TPA film (55 nm in thickness) is about 3.36 × 10^{-6} cm^2/Vs at 6.5 × 10^5 V/cm. This value is comparable to hole mobility reported for linear TPA-BT (1.46 × 10^{-6} cm^2/Vs)[21,49–51] and close to the conventional hole-transporting materials such as NPB (1.09 × 10^{-5} cm^2/Vs at 8 × 10^5 V/

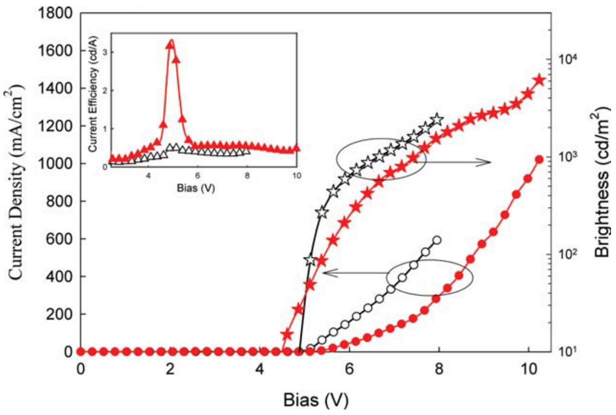

FIGURE 6 Current density versus bias and brightness versus bias characteristics of multilayer PLEDs. Device structure: ITO/PEDOT:PSS/PFO-TPA/PFO/LiF/Ca/Al; (black circle, black star, black triangle): with PFO-TPA as hole-injection layer, (white circle, white star, white triangle): without PFO-TPA layer. Inset figure shows current efficiency versus bias characteristics of the PLEDs. [Color figure can be viewed in the online issue, which is available at wileyonlinelibrary.com.]

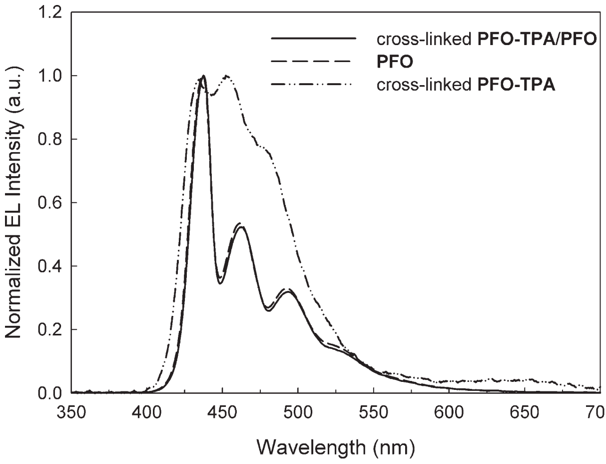

FIGURE 7 Emission spectra of light-emitting diodes using PFO or crosslinked PFO-TPA as emitting layer. Device structures: (—) ITO/PEDOT:PSS/crosslinked PFO-TPA (HIL)/PFO/LiF/Ca/Al; (–-) ITO/PEDOT:PSS/PFO/LiF/Ca/Al; (–··–) ITO/PEDOT:PSS/crosslinked PFO-TPA/Ca/Al.

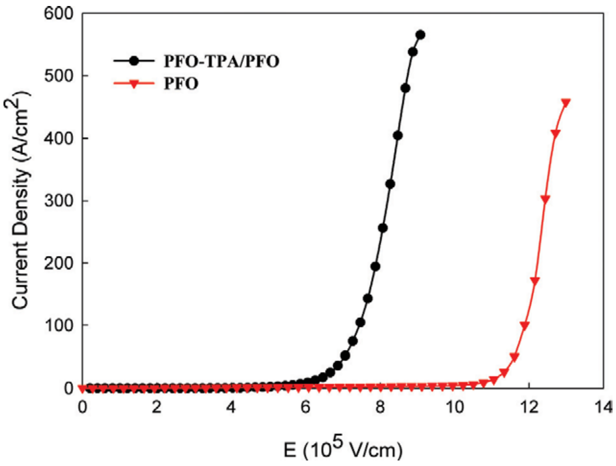

FIGURE 8 Current density versus electric field characteristics of hole-only devices using PFO as emitting layer. Device structure: ITO/PEDOT:PSS/PFO-TPA/PFO/Au/Al. [Color figure can be viewed in the online issue, which is available at wileyonlinelibrary.com.]

cm at a thickness of 100 nm).[52] Therefore, crosslinked PFO-TPA is not only an effective hole-transporting material but also highly solvent resistant to be applied in the fabrication of multilayer PLEDs by solution processes.

EXPERIMENTAL

Material

9,9-Dioctylfluorene-2,7-diboronic acid bispinacol ester,[34–36] 4-(3-methylpropyl)-*N*,*N*-bis(4-bromophenyl)aniline (**2**),[37,38] and tri(4-bromophenyl)amine (**3**)[39] were synthesized according to the procedures reported previously. Other chemicals were purchased from Aldrich, Acros, TCI, and Lancaster Chemicals and used without further purification. All the solvents such as THF and acetonitrile were dried with appropriate drying agents (Na or $CaCl_2$), then distilled under reduced pressure, and stored over 4 Å molecular sieves before use. The polymerization catalyst was tetrakis(triphenylphosphine)palladium [$Pd(PPh_3)_4$] procured from Strem.

Synthesis of *N*,*N*-bis(4-bromophenyl)-*p*-(4-vinylphenyl)aniline (5) (Scheme 1)

Tris(4-bromophenyl)amine (2 eq.), *p*-vinylphenylboronic acid (1 eq.), and $(PPh_3)_4Pd(0)$ (0.02 eq.) were dissolved in a mixture consisting of THF (20 mL), aqueous solution of K_3PO_4 (2 M) (11 mL). The mixture was first purged with Argon and stirred at 100 °C for 48 h under vigorous stirring. The cooled solution was quenched with water and extracted twice with dichloromethane. The combined organic extracts were dried ($MgSO_4$) and concentrated by rotary evaporation. Column chromatography on silica gel (EA/hexane) afforded product **5** as white solids (yield: 65%, mp: 160–161 °C).

FTIR (KBr pellet, cm^{-1}): ν 719, 815, 898, 1068, 1286, 1317, 1484, 1521, 1579, 1602, 1621, 3033, 3054, 3081. ^{1}H NMR (400 MHz, $CDCl_3$, TMS): δ 7.54–7.45 (m, 6H, Ar-H), 7.37–7.35 (d, 4H, Ar-H, $J = 8$ Hz), 7.11–7.09 (d, 2H, Ar-H, $J = 8$ Hz), 6.99–6.97 (d, 4H, Ar-H, $J = 8$ Hz), 6.78–6.71 (dd, 1H, =CH—, $J_1 = 16$ Hz, $J_2 = 16$ Hz), 5.80–5.76 (d, 1H, =CH_2, $J = 16$ Hz), 5.30–5.26 (d, 1H, =CH_2, $J = 16$ Hz). ^{13}C NMR (500 MHz, $CDCl_3$, TMS, 25 °C): δ 146.38, 146.24, 139.68, 136.45, 136.39, 135.82, 132.43, 127.88, 126.74, 126.69, 126.02, 125.63, 124.45, 115.74, 113.8. Anal Calcd for $C_{26}H_{19}Br_2N$ (%): C, 61.81; H, 3.79; N, 2.77. Found (%): C, 61.70; H, 3.85; N, 2.71. EI-MS (m/z): Calcd: 504.99; Found: 505.00.

Polymer Synthesis (Scheme 2)

The synthesis of poly(9,9-dioctylfluorene) (PFO) and copolymer PFO-TPA was carried out using a palladium-catalyzed Suzuki coupling reaction. For instance, purified 9,9-dioctylfluorene-2,7-diboronic acid bispinacol ester (**6**: 1 eq.), 4-(3-methylpropyl)-*N*,*N*-bus(4-bromophenyl)aniline (**2**: 0.9 eq.), *N*,*N*-bis(4-bromophenyl)-*p*-(4-vinylphenyl)aniline (**5**: 0.1 eq.), and $(PPh_3)_4Pd(0)$ (2.0 mol %) were dissolved in a mixture consisting of THF (22 mL) and aqueous solution of K_3PO_4 (2 M) (12 mL). The mixture was first purged with Argon and then stirred at 100 °C for 96 h under vigorous stirring. Finally, monomer **6** and 1-bromo-4-*tert*-butylbenzene were added to endcap the polymer chain. The mixture was poured into a large amount of methanol; the appeared solid was collected by filtration and washed successively with methanol, 2-propanol, and hexane, followed by Soxhlet extraction with acetone to remove trace oligomers. The residual palladium catalyst was further removed by stirring together with a silica gel (Silicycle, Si-Thiol) in toluene. Then, the solution was further extracted with DI water three times to reduce the concentration of metal ions. It was then poured into a large amount of methanol to afford light yellow fiber of PFO-TPA (yield: 70%). The resulted PFO-TPA was soluble in conventional organic solvents such as toluene, xylene, THF, and chloroform.

^{1}H NMR (400 MHz, $CDCl_3$, TMS): δ 7.76–7.74 (m, Ar-H), 7.60–7.57 (m, Ar-H), 7.26–7.14 (m, Ar-H), 6.80–6.73 (m, =CH—), 5.82–5.78 (d, =CH_2, $J = 16$ Hz), 5.29–5.26 (d, =CH_2, $J = 12$ Hz), 2.62 (br, 1H, —CH—), 2.04 (br, 4H, —CH_2—), 1.61 (br, —CH_2—), 1.28–0.74 (m, —CH_2— and —CH_3). ^{13}C NMR (500 MHz, $CDCl_3$, TMS, 25 °C): δ 151.66, 147.09, 146.67, 145.11, 143.04, 139.76, 139.41, 136.47, 136.25, 135.49, 131.83, 127.96, 127.77, 127.20, 126.73, 126.19, 125.51, 124.95, 124.57, 123.83, 120.94, 119.91, 113.6, 55.23, 41.13, 40.53, 31.80, 31.29, 30.08, 29.24, 23.85, 22.61, 21.79, 14.07, 12.32. Anal Calcd for PFO-TPA (%): C, 89.18; H, 8.79; N, 2.02. Found (%): C, 88.84; H, 8.90; N, 1.95.

Measurements

Newly synthesized compounds were identified by ^{1}H NMR, ^{13}C NMR spectroscopy, mass spectrometry, and EA. The ^{1}H NMR and ^{13}C NMR spectra were recorded with a Bruker AVANCE-300 or 400 NMR spectrometers, and the chemical shifts are reported in ppm using tetramethylsilane (TMS) as an internal standard. Mass and EA were carried out on a JEOL JMS-700 spectrometer and Heraus CHN-Rapid elemental analyzer, respectively. The Fourier transform infrared (FTIR) spectra were measured as KBr disk using a FTIR spectrometer, model 7850 from Jasco. Molecular weight and molecular weight distribution of the polymer were determined by a GPC, using THF as an eluent and monodisperse polystyrenes as calibration standards. The TGA was performed under nitrogen atmosphere using a Perkin-Elmer TGA-7 thermal analyzer; the heating rate was 20 °C/min. Thermal curing behaviors and thermal transitional properties of the polymer were investigated using a DSC, Mettler DSC 1, at a heating rate of 10 °C/min. Absorption spectra and PL spectra were measured with a Jasco V-550 spectrophotometer and a Hitachi F-4500 fluorescence spectrophotometer, respectively. Cyclic voltammograms were recorded using a voltammetric analyzer (model CV-50W from Bioanalytical Systems) under nitrogen atmosphere. The measuring cell was consisted of a polymer-coated ITO glass as the working electrode, an Ag/AgCl electrode as the reference electrode, and a platinum wire as the auxiliary electrode. The electrodes were immersed in acetonitrile containing 0.1 M (n-Bu)$_4$NClO$_4$ as an electrolyte. The energy levels were calculated using ferrocene as standard (−4.8 eV with respect to vacuum level which is defined as zero).[53,54] An AFM, equipped with a Veeco/Digital Instrument Scanning Probe Microscope (tapping mode) and a Nanoscope IIIa controller was used to examine the morphology and to estimate the thickness and RMS roughness of deposited films.

Fabrication of Light-Emitting Diodes

Multilayer LEDs with a structure of ITO/PEDOT:PSS/HIL/EML/LiF/Ca/Al were fabricated to investigate their optoelectronic characteristics. The structure means that on ITO glass, substrate are subsequently deposited with PEDOT:PSS, HIL, EML, LiF, calcium, and aluminum layers by spin coating or thermal evaporation. The ITO-coated glass substrate was washed successively in ultrasonic baths of neutral cleaner/deionized water (1:3 v/v) mixture, deionized water, acetone, and 2-propanol, followed with cleaning in a UV–Ozone chamber. A thick PEDOT:PSS layer (30 nm) was spin coated on top of the freshly cleaned ITO glass and annealed at 150 °C for 15 min in a dust-free atmosphere. The HIL was formed by spin coating a solution of PFO-TPA in toluene (10 mg/mL, 2000 rpm) on top of the PEDOT:PSS layer and crosslinked at 200 °C for 10 min under nitrogen atmosphere. The HIL solutions were filtered through a syringe filter (0.2 μm) before the spin coating. Then, the PFO (EML) was spin coated onto the HIL; the thickness of the HIL and EML were 55 and 92 nm, respectively. Finally, a thick layer of cathode was formed by successive vacuum deposition of LiF (1 nm), Ca (50 nm), and Al (100 nm) under 1×10^{-6} Torr. The luminance versus bias, current density versus bias, and emission spectral characteristics of the PLEDs were recorded using a combination of Keithley power source (model 2400) and Ocean Optics usb2000 fluorescence spectrophotometer. The fabrication of the devices was done in ambient conditions, with the following performance tests conducted in a glove box filled with nitrogen. Hole-only PLEDs were fabricated by the procedures analogous to those used for the multilayer devices, except that the top contact was Au/Al to prevent electron injection from the cathode. The device configuration was ITO/PEDOT:PSS (30 nm)/PFO-TPA (55 nm)/PFO (92 nm)/Au (50 nm)/Al (50 nm). The current versus bias characteristics of the devices were recorded using a Keithley power source (model 2400).

CONCLUSIONS

We have successfully synthesized and characterized a thermally crosslinkable hole-transporting PFO-TPA containing pendant styryl groups. Thermal decomposition and glass transition temperatures of the PFO-TPA were above 400 °C and 152 °C, respectively. After thermal crosslinking at 200 °C for 10 min, the crosslinked PFO-TPA revealed excellent solvent resistance and film morphology (RMS roughness = 0.7 nm). However, its photophysical and electrochemical properties were not greatly altered by the thermal crosslinking process. The HOMO level of crosslinked PFO-TPA (−5.30 eV) is between those of PEDOT (−5.0 ∼ −5.2 eV) and PFO (−5.8 eV), forming a stepwise energy ladder to facilitate hole injection. Multilayer PLEDs (ITO/PEDOT:PSS/PFO-TPA/PFO/LiF/Ca/Al) were successfully fabricated by successive spin-coating processes. Inserting the thermally crosslinked PFO-TPA as HIL significantly improved the device performance. Its maximum luminance and maximum luminance efficiency were 6140 cd/m^2 and 3.16 cd/A, respectively, in which the efficiency was about six times higher than that without PFO-TPA layer (0.50 cd/A). Hole-injection and hole-transport abilities of the crosslinked PFO-TPA have been successfully confirmed by the hole-only device. Our results demonstrate that the crosslinkable PFO-TPA is a promising hole-injection and hole-transport material applicable to the fabrication of multilayer PLEDs by solution processes.

The authors thank the National Science Council of Taiwan for financial aid through project NSC 98-2221-E006-002-MY3.

REFERENCES AND NOTES

1 Burroughes, J. H.; Bradley, D. D. C.; Brown, A. R.; Marks, R. N.; Mackay, K.; Friend, R. H.; Burns, P. L.; Holmes, A. B. Nature 1990, 347, 539–541.

2 Friend, R. H.; Gymer, R. W.; Holmes, A. B.; Burroughes, J. H.; Marks, R. N.; Taliani, C.; Bradley, D. D. C.; Santos, D. A. D.; Bredas, J. L.; Logdlund, M.; Salaneck, W. R. Nature 1999, 397, 121–128.

3 Tang, C. W.; VanSlyke, S. A. Appl Phys Lett 1987, 51, 913–915.

4 Kraft, A.; Grimsdale, A. C.; Holmes, A. B. Angew Chem Int Ed Engl 1998, 37, 402–428.

5 Forrest, S. R. Nature 2004, 428, 911–918.

6 Huang, F.; Cheng, Y.-J.; Zhang, Y.; Liu, M. S.; Jen, A. K.-Y. J Mater Chem 2008, 18, 4495–4509.

7 Kim, J.-S.; Friend, R. H.; Grizzi, I.; Burroughes, J. H. Appl Phys Lett 2005, 87, 023506.

8 Redecker, M.; Bradley, D. D. C.; Inbasekaran, M.; Wu, W. W.; Woo, E. P. Adv Mater 1999, 11, 241–246.

9 Morgado, J.; Friend, R. H.; Cacialli, F. Appl Phys Lett 2002, 80, 2436–2438.

10 Kulkarni, A. P.; Tonzola, C. J.; Babel, A.; Jenekhe, S. A. Chem Mater 2004, 16, 4556–4573.

11 Hughes, G.; Bryce, M. R. J Mater Chem 2005, 15, 94–107.

12 Jiang, Z.; Zhang, W.; Yao, H.; Yang, C.; Cao, Y.; Qin, J.; Yu, G.; Liu, Y. J Polym Sci Part A: Polym Chem 2009, 47, 3651–3661.

13 Jin, Y.; Lee, M.; Kim, S. H.; Song, S.; Goo, Y.; Woo, H. Y.; Lee, K.; Suh, H. J Polym Sci Part A: Polym Chem 2008, 46, 4407–4419.

14 Choulis, S. A.; Choong, V.-E.; Patwardhan, A.; Mathai, M. K.; So, F. Adv Funct Mater 2006, 16, 1075–1080.

15 Gong, X.; Wang, S.; Moses, D.; Bazan, G. C.; Heeger, A. J Adv Mater 2005, 17, 2053–2058.

16 Shi, W.; Fan, S.; Huang, F.; Yang, W.; Liu, R.; Cao, Y. J Mater Chem 2006, 16, 2387–2394.

17 Chen, J. P.; Klaerner, G.; Lee, J. I.; Markiewicz, D.; Lee, V. Y.; Miller, R. D.; Scott, J. C. Synth Met 1999, 107, 129–135.

18 Liu, S.; Jiang, X.; Ma, H.; Liu, M. S.; Jen, A. K. Y. Macromolecules 2000, 33, 3514–3517.

19 Jiang, X. Z.; Liu, S.; Liu, M. S.; Herguth, P.; Jen, A. K. Y.; Fong, H.; Sarikaya, M. Adv Funct Mater 2002, 12, 745–751.

20 Niu, Y.-H.; Liu, M. S.; Ka, J.-W.; Jen, A. K. Y. Appl Phys Lett 2006, 88, 093505.

21 Paul, G. K.; Mwaura, J.; Argun, A. A.; Taranekar, P.; Reynolds, J. R. Macromolecules 2006, 39, 7789–7792.

22 Niu, Y.-H.; Liu, M. S.; Ka, J.-W.; Bardeker, J.; Zin, M. T.; Schofield, R.; Chi, Y.; Jen, A. K.-Y. Adv Mater 2007, 19, 300–304.

23 Cheng, Y.-J.; Liu, M. S.; Zhang, Y.; Niu, Y.; Huang, F.; Ka, J.-W.; Yip, H.-L.; Tian, Y.; Jen, A. K.-Y. Chem Mater 2008, 20, 413–422.

24 Liu, M. S.; Niu, Y.-H.; Ka, J.-W.; Yip, H.-L.; Huang, F.; Luo, J.; Kim, T.-D.; Jen, A. K. Y. Macromolecules 2008, 41, 9570–9580.

25 Krishnan, R. S.; Mackay, M. E.; Duxbury, P. M.; Pastor, A.; Hawker, C. J.; Van Horn, B.; Asokan, S.; Wong, M. S. Nano Lett 2007, 7, 484–489.

26 Lim, B.; Hwang, J.-T.; Kim, J. Y.; Ghim, J.; Vak, D.; Noh, Y.-Y.; Lee, S.-H.; Lee, K.; Heeger, A. J.; Kim, D.-Y. Org Lett 2006, 8, 4703–4706.

27 Zhang, Y.-D.; Hreha, R. D.; Jabbour, G. E.; Kippelen, B.; Peyghambarian, N.; Marder, S. R. J Mater Chem 2002, 12, 1703–1708.

28 Bacher, E.; Bayerl, M.; Rudati, P.; Reckefuss, N.; Muller, C. D.; Meerholz, K.; Nuyken, O. Macromolecules 2005, 38, 1640–1647.

29 Akhrass, S. A.; Gal, F.; Damiron, D.; Alcouffe, P.; Hawker, C. J.; Cousin, F.; Carrot, G.; Drockenmuller, E. Soft Matter 2009, 5, 586–592.

30 Lee, S.; Lee, B.; Kim, B. J.; Park, J.; Yoo, M.; Bae, W. K.; Char, K.; Hawker, C. J.; Bang, J.; Cho, J. J Am Chem Soc 2009, 131, 2579–2587.

31 Akhrass, S. A.; Damiron, D.; Carrot, G.; Drockenmuller, E. J Polym Sci Part A: Polym Chem 2010, 48, 3888–3895.

32 Zhu, K.; Iacono, S. T.; Budy, S. M.; Jin, J.; Smith, D. W. J Polym Sci Part A: Polym Chem 2010, 48, 1887–1893.

33 Adachi, C.; Nagai, K.; Tamoto, N. Appl Phys Lett 1995, 66, 2679–2681.

34 Belletete, M.; Beaupre, S.; Bouchard, J.; Blondin, P.; Leclerc, M.; Durocher, G. J Phys Chem B 2000, 104, 9118–9125.

35 Gautrot, J. E.; Hodge, P. Polymer 2007, 48, 7065–7077.

36 Gautrot, J. E.; Hodge, P.; Helliwell, M.; Raftery, J.; Cupertino, D. J Mater Chem 2009, 19, 4148–4156.

37 Wenseleers, W.; Stellacci, F.; Meyer-Friedrichsen, T.; Mangel, T.; Bauer, C. A.; Pond, S. J. K.; Marder, S. R.; Perry, J. W. J Phys Chem B 2002, 106, 6853–6863.

38 Changkun, L.; Amanda, R.; Bing, Z. J Polym Sci Part A: Polym Chem 2008, 46, 7268–7272.

39 Lee, H. J.; Sohn, J.; Hwang, J.; Park, S. Y.; Choi, H.; Cha, M. Chem Mater 2004, 16, 456–465.

40 Qiu, Y.; Qiao, J. Thin Solid Films 2000, 372, 265–270.

41 Tang, C. W.; VanSlyke, S. A.; Chen, C. H. J Appl Phys 1989, 65, 3610–3616.

42 Morgado, J.; Cacialli, F.; Friend, R. H.; Iqbal, R.; Yahioglu, G.; Milgrom, L. R.; Moratti, S. C.; Holmes, A. B. Chem Phys Lett 2000, 325, 552–558.

43 Liao, J. L.; Chen, X.; Liu, C. Y.; Chen, S. A.; Su, C. H.; Su, A. C. J Phys Chem B 2007, 111, 10379–10385.

44 Chen, R.-T.; Chen, S.-H.; Hsieh, B.-Y.; Chen, Y. J Polym Sci Part A: Polym Chem 2009, 47, 2821–2834.

45 Weinfurtner, K.-H.; Fujikawa, H.; Tokito, S.; Taga, Y. Appl Phys Lett 2000, 76, 2502–2504.

46 Malliaras, G. G.; Salem, J. R.; Brock, P. J.; Scott, C. Phys Rev B 1998, 58, 13411.

47 Martens, H. C. F.; Brom, H. B.; Blom, P. W. M. Phys Rev B 1999, 60, 8489.

48 Chu, T.-Y.; Song, O.-K. Appl Phys Lett 2007, 90, 203512.

49 Chiatzun, G.; Kline, R. J.; Michael, D. M.; Ekaterina, N. K.; Jean, M. J. F. Appl Phys Lett 2005, 86, 122110–122112.

50 Yang, Z.; Xu, B.; He, J.; Xue, L.; Guo, Q.; Xia, H.; Tian, W. Org Electron 2009, 10, 954–959.

51 He, C.; He, Q.; Yi, Y.; Wu, G.; Bai, F.; Shuai, Z.; Li, Y. J Mater Chem 2008, 18, 4085–4090.

52 Lu, Z.; Deng, Z.; Zheng, J.; Zou, Y.; Chen, Z.; Xu, D.; Wang, Y. Phys E 2009, 41, 1806–1809.

53 Rusling, J. F.; Suib, S. L. Adv Mater 1994, 6, 922–930.

54 Liu, Y.; Liu, M. S.; Jen, A. K.-Y. Acta Polym 1999, 50, 105–108.